Schweizerische Eidgenossenschaft
Confédération suisse
Confederazione Svizzera
Confederaziun svizra

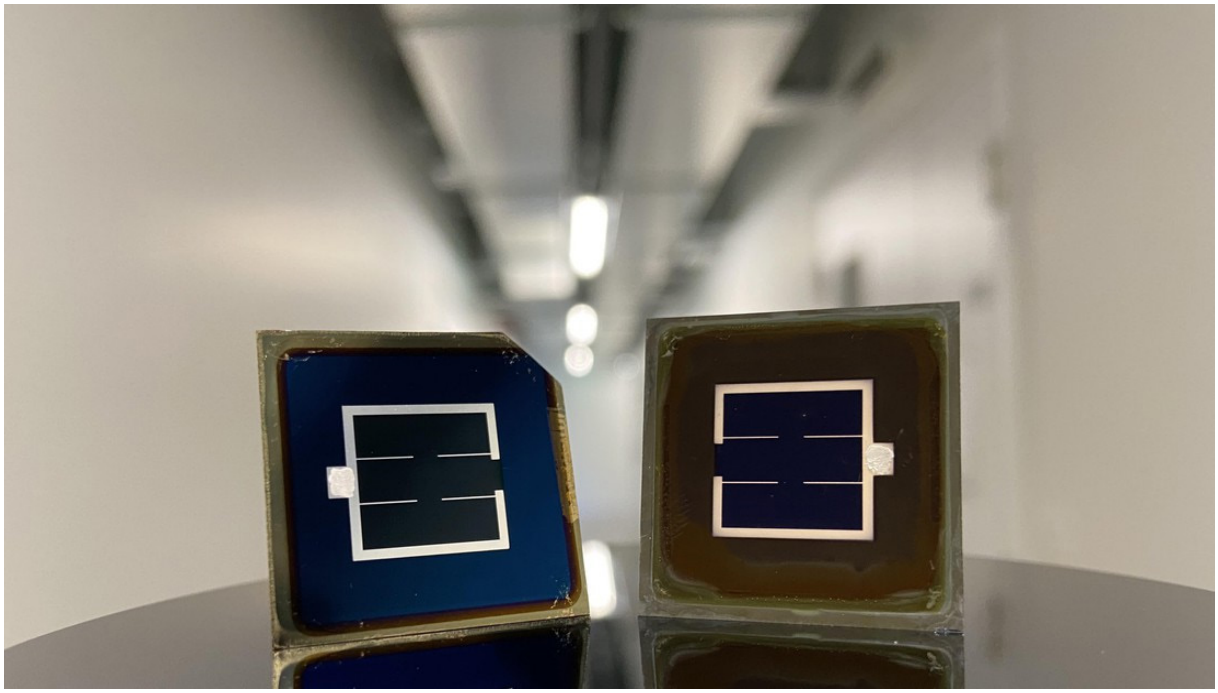
Federal Department of the Environment,
Transport, Energy and Communications DETEC

Swiss Federal Office of Energy
Energy Research and Cleantech

Final report from 21 October 2024

PRESTO

Perovskite/silicon tandem solar cells with high fill factors



Source: Deniz Turkay, 2022

Publisher:
Swiss Federal Office of Energy SFOE
Energy Research and Cleantech
CH-3003 Berne
www.energy-research.ch

Co-financing:
SNSF EPISODE
SNSF PAPET
Bridge POWER
SFOE INTENT

Subsidy recipients:
EPFL STI IEM PV-LAB, MC A2 304 (Microcity), Rue de la Maladière 71b, CH-2002 Neuchâtel 2

Authors:
Christian Wolff, EPFL STI IEM PVLAB, christian.wolff@epfl.ch
Aïcha Hessler-Wyser, EPFL STI IEM PVLAB, aicha.hessler@epfl.ch
Christophe Ballif, EPFL STI IEM PVLAB, Christophe.ballif@epfl.ch

SFOE project coordinator:
Stefan Oberholzer, stefan.oberholzer@bfe.admin.ch

SFOE contract number: SI/502209-01

The authors bear the entire responsibility for the content of this report and for the conclusions drawn therefrom.

Summary

Perovskite solar cells have developed so rapidly in a short period of time that commercialization can be expected soon. Especially in combination with already established silicon solar cells as a tandem, they promise high efficiencies at low costs. At the beginning of the PRESTO project, the maximum efficiency of this technology was approximately at the theoretical limit of silicon cells alone (approx. 29%). The goal of PRESTO was to minimize recombination and absorption losses by successively improving the passivation layers of the perovskite solar cell and their optimized deposition on pseudo-random silicon textures. In particular the development of the contact displacement via a thin tunneling layer of AlOx - enabling reduced losses at the electron contact - was achieved in the project alongside two additional passivating interlayers/ partial contacting schemes (pFBPA, SiOx nanparticles). A target efficiency of > 30% and then > 31% was achieved for the first time, resulting in a double world record (In fact three records: 29.9%, 30.9%, 31.25%). The stability of these cells was further evaluated, but currently appears to be insufficient for commercial applications.

Zusammenfassung

Perowskit Solarzellen haben sich innert kürzester Zeit derart entwickelt, dass von einer zeitnahen Kommerzialisierung auszugehen ist. Insbesondere in Kombination mit bereits etablierten Siliziumsolarzellen als Tandem versprechen sie hohe Wirkungsgrade bei geringen Kosten. Zu Beginn des Projektes PRESTO lag der maximale Wirkungsgrad dieser Technologie etwa bei dem theoretischen Limit von Siliziumzellen alleine (ca. 29%). Ziel von PRESTO war es durch sukzessive Verbesserung der Passivierungsschichten der Perowskitsolarzelle und deren optimierten Abscheidung auf pseudozufällige Silizumtexturen die Rekombinations- und Absorptionsverluste zu minimieren. Dies wurde insbesondere mittels dreier Methoden realisiert: Ein ultradünnes Tunneloxid aus AlOx erlaubt die Abstandsregulierung zwischen Perowskit und Elektronenkontakt und damit die Verringerung der Verluste an jenem Kontakt; ferner wurden zwei weiter Schichten entwickelt: eine passivierende Schicht und ein partieller Kontakt (pFBPA, SiOx Nanopartikel). Mithilfe dieser Methoden konnte das Ziel eines Wirkungsgrades von > 30% und dann > 31% erreicht werden, was zu einem doppelten Weltrekord führte (im Grunde dreifach: 29.9%, 30.9%, 31.25%). Die Stabilität dieser Zellen wurde weiter evaluiert, diese erscheint jedoch gegenwärtig noch unzureichend für kommerziellen Anwendungen.

Résumé

Les cellules solaires pérovskites ont connu un développement si rapide en peu de temps que leur commercialisation est envisageable prochainement. En particulier, en combinaison avec les cellules solaires en silicium déjà établies en tandem, elles promettent des rendements élevés à faibles coûts. Au début du projet PRESTO, le rendement maximal de cette technologie était approximativement à la limite théorique des cellules en silicium seules (environ 29%). L'objectif de PRESTO était de minimiser les pertes par recombinaison et absorption en améliorant successivement les couches de passivation de la cellule solaire pérovskite et leur dépôt optimisé sur des textures de silicium pseudo-aléatoires. En particulier, le développement du déplacement de contact via une couche mince d'AlOx qui permet l'effet tunnel - permettant de réduire les pertes au niveau du contact négative - a été réalisé dans le projet, parallèlement à deux autres couches intermédiaires de passivation/systèmes de contact partiel (pFBPA, nanoparticules de SiOx). Une efficacité de > 30% et puis > 31% a été atteint pour la première fois, ce qui a donné lieu à un double record mondial (en fait, trois records : 29.9%, 30.9 %, 31.25 %). La stabilité de ces cellules a été évaluée plus en détail, mais elle semble actuellement insuffisante pour les applications commerciales.

Main findings («Take-Home Messages»)

- Perovskite-silicon tandem solar cells can be fabricated using standard silicon textures with comparable high efficiencies to the more established flat analogues
- > 31% power conversion efficiency was achieved on small area devices, allowing for up to 30% reduced electricity prices assuming similar lifetimes
- Operational stability however is still to be improved before commercial applications are foreseeable
- Results sparked worldwide interest with now large industrial players entering the field (HANWHA QCELLS, Jinko Solar, LONGi, FirstSolar, Meyer-Burger)

Contents

Summary ... **3**
Zusammenfassung ... **3**
Résumé ... **3**
Main findings («Take-Home Messages») ... **4**
Contents ... **5**
List of figures ... **6**
List of abbreviations ... **7**
1 Introduction ... **8**
1.1 Context and motivation ... 8
1.2 Project objectives ... 8
2 Approach, method, results and discussion ... **9**
2.1 Approach & methods ... 9
2.2 Results & Discussion ... 11
2.2.1. Single-Junction devices on Si-texture-replicas and rough substrates based on LPCVD ZnO 11
2.2.2. Contact layer selection and passivation layers ... 14
3 Conclusions and outlook ... **19**
4 National and international cooperation ... **20**
5 Publications and other communications ... **20**
6 References ... **21**

List of figures

Figure 1: Evolutionary workflow of PRESTO. The orange arrows indicate the illumination direction. The acronyms are as follows: ITO – indium tin oxide, ETL – electron transporting layer, PK – perovskite, HTL – hole transporting layer, RJ – recombination junction, Rep – Replicated.

Figure 2: UV NIL process for replicating micrometer-sized pyramids. A) process to create inverted pyramid polymer textures on glass. B) process to fabricate regular pyramid polymer textures on glass. C) top view image of ITO-coated polymer film featuring inverted pyramids (scalebar 4 um). D) standard regular pyramids of a Si wafer (scalebar 4 um). 12

Figure 3: Replicated Si textures. A) photograph of a fully textured perovskite solar cell. The top part of the substrate was not covered with the UV-cured textured polymer, hence exhibiting the reflective appearance of a flat Ag film. B) (top) EQE of good performing fully textured solar cells featuring replicas with regular or inverted pyramid. (bottom) JV of top-performing solar cell fabricated using inverted pyramids. 13

Figure 4: ZnO-modified perovskite solar cells. A) growth manipulation of ZnO-favoring a- or c-axis growth or an in-between, mixed growth allowing for facile fabrication of perovskite solar cells featuring structured substrates. B) cross-sectional SEM image of a perovskite solar cell on top of said ZnO layer featuring a protective Al2O3 interlayer. C) JV and implied JV (iJV) curves of planar and ZnO-modified samples. D) Corresponding EQE curves of said devices. Results from[10]. 14

Figure 5: PLQY loss analysis for hybrid-deposited perovskite absorbers in contact with different HTLs (reference on glass, spiro-TTB, TaTm, Me-4PACz), with and without additive for passivation (FBPAc) and in contact with the ETL (C60). 15

Figure 6: A) JV scans of tandem devices with a perovskite top-cell featuring TaTm or Me-4PACz as HTL in forward and reverse scan (dashed and full line, resp.). B) Fill-factor statistics of such tandem devices. 16

Figure 7: A) time-line of perovskite/silicon tandem solar cells fabricated by PV-LAB and certified (red) along with the world record at the time (HZB, 29.8%). The arrows around highlight some of the innovations that led to the different results. In detail: B) FF x VOC product of the perovskite top cell with and without an ALD-deposited AlOx interlayer. C) top and bottom view SEM images of SiOx nanoparticles on ITO/Me-4PACz and embedded in the peeled perovskite creating a partial contact at the HTL interface. D) bulk and interface passivation via partial contact by admixing FBPAc into the organohalide mix for creating the perovskite in a two-step method. E) Photographs with top electrode/TCO design featuring one and three fingers. F) Efficiency evolution of the front-flat tandem devices as a function of batch number highlighting the different developments. In grey are batches with known flaws (e.g., failed depositions or similar) which still allowed for overall improvements. 17

Figure 8. Stability measurements. A) storage stability (N2, dark) of fully textured tandem devices shown in some cases (here three different batches are compared) no degradation over the course of a year (red, blue) whereas others degraded slightly (black, 80% retention). B) operational stability at 25°C (pink, grey (from 2018 Nat. Mater.)) and 65°C (black, red, blue) reaching T90 of 35 and 20h at room temperature and 65°C, respectively. C) day-night cycle (12h MPP at 25°C in ambient 50% RH, 12h rest in dark at room temperature) of a front-side polished tandem. D) best continuous MPP at 25°C in ambient air with an initial burn-in for 12h and then a comparably low degradation rate of 1.2×10^{-4} h^{-1} corresponding to a projected T90 of ca. 830 h, assuming a linear degradation, which corresponds to only 80% of the targeted stability. 18

List of abbreviations

SFOE	Swiss Federal Office of Energy
ITO	Indium Tin Oxide
IZO	Indium Zinc Oxide
IZrO	Indium Zirconium Oxide
TCO	Transparent Conductive Oxide
UV	Ultraviolet
NIL	Nano Imprint Lithography
PV	Photovoltaic
PLQY	Photoluminescence quantum yield

1 Introduction

1.1 Context and motivation

The rapid growth of utility-scale photovoltaics (PV) has positioned it as the cheapest form of electricity in many regions. However, to truly dominate the energy landscape and displace fossil fuels, further advancements in PV technology are crucial. While crystalline silicon (c-Si) based solar cells have reached a high level of maturity, their efficiency is approaching fundamental limits and further cost reductions are becoming increasingly difficult.

This necessitates a paradigm shift towards more sophisticated solar cell designs, particularly multi-junction configurations. Among these, perovskite/c-Si tandem solar cells hold immense promise due to their potential for high efficiency exceeding 30%, utilization of earth-abundant materials, and compatibility with existing c-Si technology.

This motivates developing perovskite/c-Si tandems because:

- Overcoming the efficiency limitations of single-junction c-Si solar cells: Tandem configurations allow for a more efficient utilization of the solar spectrum, paving the way for significant efficiency gains beyond the theoretical limits of c-Si.
- Significant cost reduction potential: While tandem cells are inherently more complex, the cost increase is largely offset by the balance-of-systems cost at the system level. Higher efficiency translates directly into lower electricity costs.
- Sustainable and scalable technology: Perovskites are made from earth-abundant materials and can be processed using low-cost techniques, ensuring a sustainable and scalable solution for future energy needs.
- Urgency of climate change mitigation: The rapid decarbonization of our energy supply requires accelerated deployment of renewable energy sources, and highly efficient perovskite/c-Si tandems can play a pivotal role in this transition.

Specifically for Switzerland, the development of high-performance PV products is particularly relevant due to the

- inherent space constraints: High-efficiency modules are crucial for maximizing energy generation from limited rooftop areas and preserving valuable land resources.
- Economic benefits for Swiss companies: Several Swiss companies (INDEOtec SA, PASAN SA, MB group, Fluxim AG) are active in the PV industry and stand to benefit from advancements in perovskite/c-Si tandem technology through licensing and tool development.

1.2 Project objectives

PRESTO's objectives focused on achieving high-efficiency perovskite/silicon tandem solar cells, specifically exceeding 30% efficiency. A key objective was to systematically investigate the performance impact of transitioning from planar to textured substrates and optimizing each subsequent layer and corresponding process step.

Here, the aim was to identify and select high-performing hole-transporting materials that enable excellent open-circuit voltage and fill factor characteristics in first planar devices on sub-square centimeter scale before scaling to 1cm2 and demonstrating high-efficiency devices on textured substrates, minimizing performance loss compared to planar counterparts and maintaining high fill factors > 80%.

The project thereafter aimed to optimize the entire tandem top-stack structure, e.g., including the metallization design and expand the device area towards dimensions suitable for industrial wafer sizes while

preserving performance metrics. Combined, the project aimed to achieve fully textured perovskite-silicon tandem devices exhibiting high open-circuit voltage > 1.9V, short-circuit current densities > 20 mA/cm2, and fill factors in excess of 80%, culminating in efficiencies exceeding 30% for cells with an active area > 1cm2 and demonstrating long-term stability under operational conditions.

2 Approach, method, results and discussion

2.1 Approach & methods

The PRESTO project embarked on an ambitious endeavor to unlock the full potential of perovskite/c-Si tandem solar cells, aiming to surpass the 30% efficiency milestone. Recognizing the inherent complexities associated with these devices, particularly when fabricated on textured c-Si substrates renowned for their superior light management properties, we adopted a meticulously detailed, deconstructive approach.

This approach, akin to a meticulous surgical dissection, involved systematically breaking down the fabrication process into discrete, manageable stages. Rather than confronting the full complexity of the tandem structure head-on, we began with a simple planar single-junction perovskite cell as our foundation, progressively introducing each layer and process step required to construct a fully functional textured tandem device.

This methodical, step-by-step progression served as a powerful lens through which we could isolate and scrutinize the impact of each individual component and process on the overall device performance. Our primary focus was on the fill factor (FF), a critical parameter often limiting the efficiency of textured tandems. By meticulously unravelling the nuanced interplay between materials and processes at each stage, we aimed to pinpoint and mitigate FF losses, paving the way for highly efficient and stable devices.

Our investigation was structured into two distinct work packages, detailed below, with the planned step-by-step approach detailed in Figure 1.

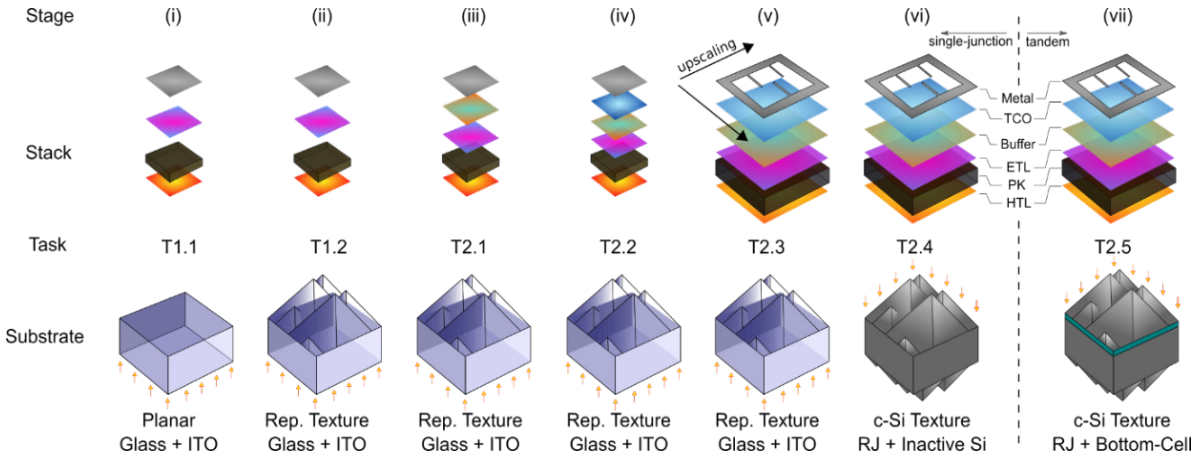


Figure 1: Evolutionary workflow of PRESTO. The orange arrows indicate the illumination direction. The acronyms are as follows: ITO – indium tin oxide, ETL – electron transporting layer, PK – perovskite, HTL – hole transporting layer, RJ – recombination junction, Rep – Replicated.

Work package 1: From Flat to Textured Single-Junction Solar Cells: Laying the Foundation for Success

This initial phase centered on mastering the fundamental transition from planar to textured substrates. We embarked on a rigorous investigation into the influence of texture properties on perovskite film quality and overall cell performance. The primary objective was to maximize FF and efficiency on textured substrates before incorporating the complexities of the full tandem structure. This involved establishing a high-performance baseline with planar single-junction cells. Utilizing a hybrid perovskite deposition process involving thermal evaporation of lead and cesium halides followed by spin-coating of organic halides, we fabricated planar single-junction cells on ITO-coated glass substrates. We optimized the perovskite composition and device architecture to achieve high FF and efficiency, serving as a critical benchmark for subsequent textured device fabrication.

We then replicated the high-performance baseline on textured substrates. We replicated the random pyramidal textures of c-Si onto glass substrates using imprint lithography, subsequently coating them with ITO to form the bottom electrode. Fabricating perovskite single-junction cells on these textured substrates allowed us to identify challenges related to perovskite growth and morphology on non-planar surfaces. We explored various strategies to overcome these challenges, including varying perovskite thickness to investigate the impact of perovskite layer thickness on device performance, considering factors such as height discrepancies between pyramid peaks and valleys, bulk transport limitations, and perovskite conversion efficiency. We also implemented a multi-step conversion process, repeating the deposition and conversion sequence to enhance perovskite crystallization and mitigate potential issues related to insufficient interdiffusion of species in thicker films. Finally, we explored different morphological levers, investigating techniques to modulate perovskite morphology, such as varying template deposition parameters, adding chemical agents during crystallization, and exposing the perovskite to solvent or organic halide vapors.

Work package 2: From Textured Single-Junctions to Textured Tandems: A Step-by-Step Ascent Towards High Efficiency

Building upon the foundation established in work package 1, this phase focused on systematically integrating each component of the tandem structure, analyzing the impact of each addition on device performance. This involved adding the buffer layer, a SnO_2 layer deposited by atomic layer deposition (ALD) to protect the perovskite layer from subsequent sputtering damage during transparent conductive oxide (TCO) deposition. We carefully investigated the effects of ALD processing on perovskite film quality, exploring strategies to mitigate potential damage, such as optimizing ALD parameters like precursor pulse lengths, purge times, and deposition temperatures to minimize precursor penetration and reactions with the underlying perovskite layer. We also explored the use of nucleation layers to promote uniform and conformal growth of the SnO_2 buffer layer, potentially limiting precursor penetration into the perovskite. Furthermore, we investigated doping strategies to enhance the conductivity of the SnO_2 buffer layer, mitigating potential transport limitations.

Next, we added the TCO layer, depositing a sputtered IZO TCO layer on top of the buffer layer to facilitate front-side illumination. We assessed the impact of sputtering damage on the underlying layers and optimized the TCO/buffer layer interface to maintain high FF, exploring alternative TCO materials and surface treatments as needed.

Subsequently, we focused on opening the window, co-optimizing the TCO and metallization pattern by transitioning from full-area metallization to partial-area grids to allow for front-side illumination. This step involved scaling up the device area to dimensions relevant for industrial metallization, addressing challenges related to ohmic losses in the TCO and metal fingers, and ensuring layer uniformity over larger areas.

Then, we moved from glass to Si, introducing the recombination junction. We replaced the glass substrate with a c-Si substrate, incorporating a recombination junction to facilitate charge carrier transport between the perovskite top cell and the c-Si bottom cell. We investigated different recombination junction materials and designs, analyzing their impact on perovskite growth, interface properties, and overall device performance.

Finally, we added the bottom cell, integrating a c-Si bottom cell and carefully optimizing its performance under half-sun illumination conditions to ensure proper current matching with the perovskite top cell. We addressed challenges related to edge effects in small-scale c-Si cells and fine-tuned the perovskite bandgap to achieve optimal current matching.

Throughout this comprehensive investigation, we employed a diverse arsenal of characterization techniques, including scanning electron microscopy (SEM) to visualize the morphology and microstructure of the perovskite films and interfaces, X-ray diffraction (XRD) to analyze the crystal structure and phase purity of the perovskite materials, photoluminescence (PL) to assess the optoelectronic quality of the perovskite films and identify potential defects, current-voltage (J-V) measurements to determine the key performance parameters of the solar cells, including efficiency, FF, open-circuit voltage, and short-circuit current, lock-in thermography to visualize current flow and identify potential shunting pathways, illumination-dependent photoluminescence to further assess the recombination orders and shunting due to potential defects, and ultraviolet and X-ray photoemission spectroscopy (UPS/XPS) to analyze the electronic structure and energy level alignment at interfaces. We also utilized atomic force microscopy (AFM) to characterize the surface topography and roughness of the various layers.

This detailed and systematic approach allowed us to unravel the intricate complexities of textured perovskite/c-Si tandem solar cells, providing a comprehensive understanding of the factors influencing device performance. By meticulously dissecting the fabrication process and systematically optimizing each component and process step, we successfully navigated the challenges associated with this promising technology, paving the way for the development of highly efficient and stable tandem solar cells that hold the key to a sustainable energy future.

2.2 Results & Discussion

2.2.1. Single-Junction devices on Si-texture-replicas and rough substrates based on LPCVD ZnO

In the initial works we sought to establish a platform on which we could develop the perovskite top cell which mimicked the scenario in the tandem as closely as possible. To this end we had two fundamental options, where we then established a third option, as described below:

1. Replicate the micrometer-sized structures of KOH-etched c-Si wafers using non-absorbing polymer resins and fabricate substrate opaque or superstrate semi-transparent devices
2. Progress without front-side texture for tandem devices with a mechanochemically polished front side and textured rear-side, here standard commercial ITO substrates are the optimal platform
3. Fabricate substrates with pyramids structured < 1 micrometer which allow for semi-conformal or buried textures

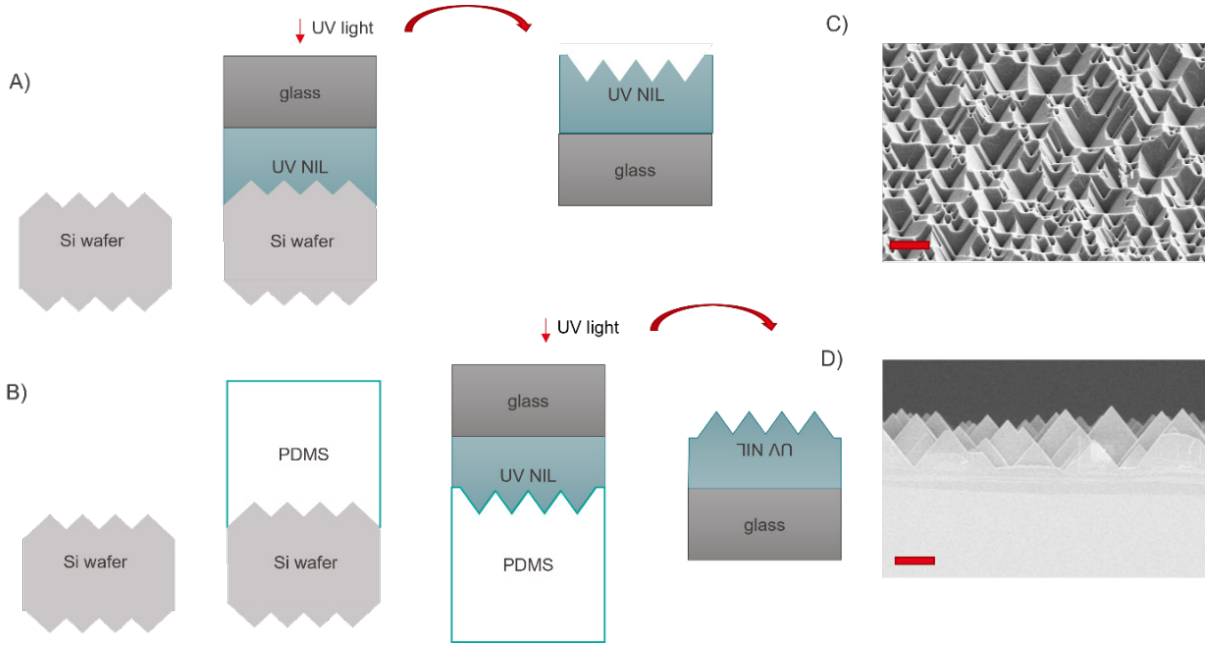


Figure 2: UV NIL process for replicating micrometer-sized pyramids. A) process to create inverted pyramid polymer textures on glass. B) process to fabricate regular pyramid polymer textures on glass. C) top view image of ITO-coated polymer film featuring inverted pyramids (scalebar 4 um). D) standard regular pyramids of a Si wafer (scalebar 4 um).

We explored all three options. For **option 1**. we used knowledge acquired in the lab from previous projects on thin-film silicon solar cells, but adopted the processes to the larger pyramid sizes.[1] In z particular, we fabricated textured substrates with regular or inverted pyramids by adhering a UV-curable polymer film (spincoated on glass) directly to a textured Si wafer (modified with a fluorosilane) creating inverted pyramids, or using a pre-fabricated stamp (PDMS) to generate positive pyramids.

After forming the substrates with the polymer resin, ITO was deposited via RF sputtering. For high-quality ITO (= high transparency and high mobility), typically an annealing step at ca 300 °C is necessary. The polymer however, decomposes at temperatures > 150 °C so that we had to accept lower performing TCOs. In particular, we accepted low transparency in the UV-blue part of the spectrum in order to allow for sufficiently low resistive losses. Other than that the perovskite solar cell was formed by spincoating a SAM as HTL (MeO-2PACz) and the perovskite was formed via the hybrid PVD-solution route[2] (CsBr /PbI2 co-evaporated and afterwards converted via solution processing the organohalide). The device was further terminated by thermal evaporation of C60, ALD-deposited SnO2 and thermally evaporated Ag. MgFx was deposited on the glass side as an antireflective coating. In Figure 3a a photograph of such a device can be seen with a textured and non-textured, highly reflective region. Exemplary device EQE and JV curve are shown, too, with comparable, excellent optical performance for either regular or inverted textures and peak performances ~19%. The remaining optical losses stem primarily from the rather absorptive ITO (parasitic absorption < 500 nm). Similarly, the Voc is recombination limited (no additives or interface passivation at this point). Similarly, the FF is impacted due to non-radiative recombination and the comparable high sheet resistance of the TCO (~40 Ohm sqr vs. 15 Ohm sqr for commercial ITO). Despite these predictable short-comings, the developed system could serve as a platform for further developments.

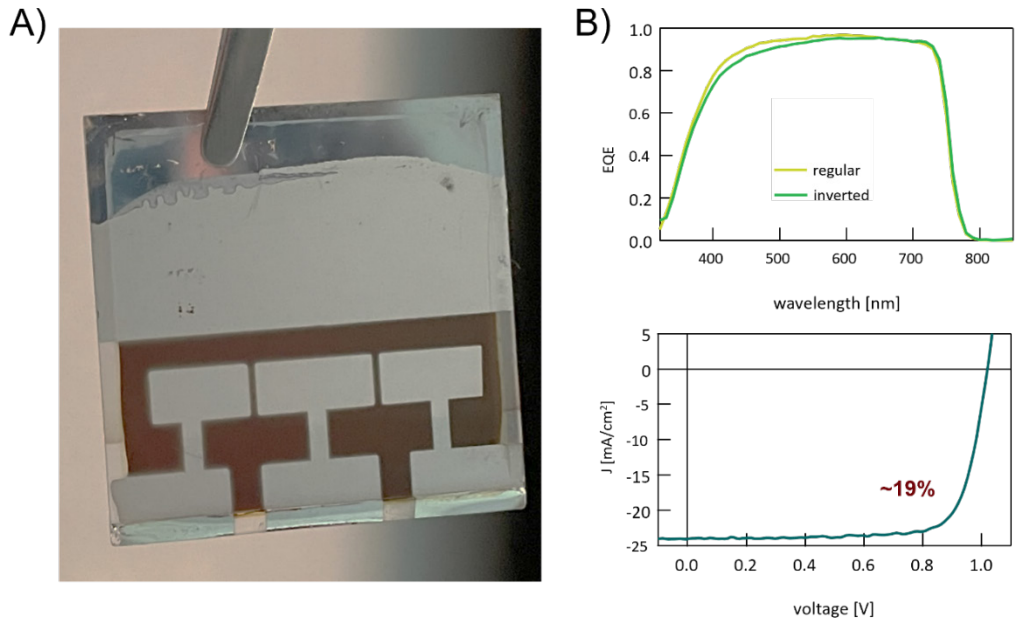


Figure 3: Replicated Si textures. A) photograph of a fully textured perovskite solar cell. The top part of the substrate was not covered with the UV-cured textured polymer, hence exhibiting the reflective appearance of a flat Ag film. B) (top) EQE of good performing fully textured solar cells featuring replicas with regular or inverted pyramid. (bottom) JV of top-performing solar cell fabricated using inverted pyramids.

Option 2 required no further modifications for a standard substrate, commercial ITO substrates allow are readily in place.

Option 3: While researching the methods to replicate nanostructures we stumbled across further examples of random structures with texture sizes below the typical 2-5 micrometer (Figure 2d). With new literature reports suggesting that upon modification of the texturization receipes[3–6], Si wafer texturing can be modified to exhibit sub-micrometer textures we further investigated substrates with similar properties. Previous projects in the lab revolved around the fabrication of a-Si and/or microcrystalline Si thin-film solar cells, where often a LPCVD grown ZnO layer was used as a contact with near Lambertian light scattering properties.[7] Inspired by this we aimed to use this process to fabricate layer with < 1um textures, which would further enable to likewise solution-process perovskites on textures. First attempts rendered ZnO layers with tuneable roughness depending on the growth temperature and precursor fluxes, favoring growth along the wurtzite a- or c-axis of ZnO, Figure 4a. We chose the intermediate based on preliminary SEM and AFM characterization, suggesting compatibility with hybrid, and also fully solution-processed perovskite layers with texture sizes well below 1 um in the mixed growth case. To validate that devices could be fabricated atop the ZnO, similar to the polymeric texture replicas, ITO was deposited and devices fabricated. These showed to be non-functional where the perovskite absorber rapidly degraded forming a yellow, decomposed film. This observation is not new, as ZnO is known to rapidly decompose organohalide perovskites[8]. Surprisingly the ITO layer only mildly decelerated the process (we observed a similar decomposition at the boundary, where ITO was masked to allow for contacting of the top-contact). In order to chemically isolate the ZnO and perovskite layer we added a 50 nm thick high-temperature Al2O3 layer grown via ALD, Figure 4b. With this “sealing” and the optimized roughness, allowing for solution or hybrid processed halide perovskites we fabricated analogous to above devices and characterized them with JV and EQE measurements (Figure 4c,d). The rough ZnO resulted in two major differences to the EQE, when compared to the planar reference devices. First, the mild interference fringes are removed and the overall EQE is enhanced in the spectral band between 500 and 800 nm. At the same time the EQE <400 nm is fully suppressed, since this light is (parasitically) absorbed by the electronically inactive ZnO. This reduction in photogenerated current is overcompensated by the improved current in the visible band, as described above, resulting in an overall 1mA/cm2 improved current. Furthermore, the UV filter is likely to improve the often-reported instability of halide perovskites when exposed to UV illumination.

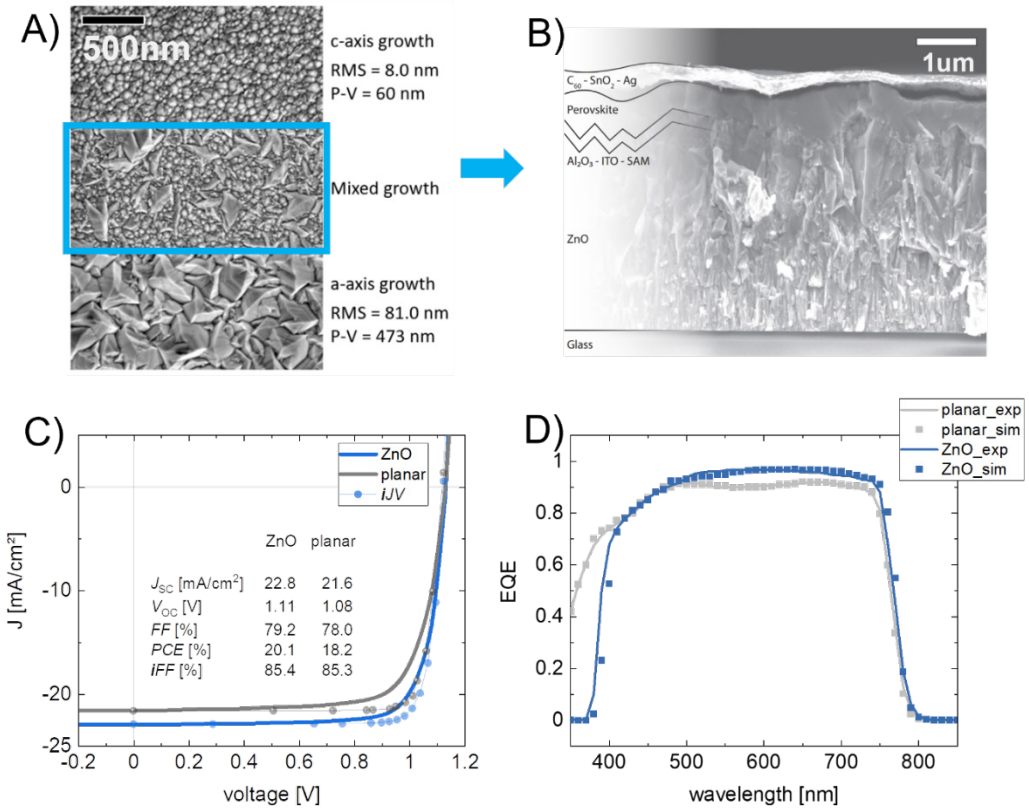


Figure 4: ZnO-modified perovskite solar cells. A) growth manipulation of ZnO-favoring a- or c-axis growth or an in-between, mixed growth allowing for facile fabrication of perovskite solar cells featuring structured substrates. B) cross-sectional SEM image of a perovskite solar cell on top of said ZnO layer featuring a protective Al2O3 interlayer. C) JV and implied JV (iJV) curves of planar and ZnO-modified samples. D) Corresponding EQE curves of said devices. Results from[10].

Over the course of these initial screening experiments, we likewise fabricated so-called “fake-tandems”, where, by fabricating unipolar devices, the Si bottom cell acts as an electrode and is as a solar cell by itself inactive, i.e., ITO/a-Si(n+)/c-Si(n)/a-Si(n+)/ITO/Ag. This corresponds to the devices schematically shown in the plan as T2.4. Given the comparably small batch size we could fabricate and the numerous steps involved in the fabrication of the replica and ZnO-based cells (preparation of Si wafer, surface functionalization, stamp preparation, glass substrate cleaning, replication, curing, ITO deposition or alternatively to stamp fabrication: LPCVD and ALD deposition) and comparably small batch sizes (typically only 20 substrates in one batch, one person, full day) compared to the available Si fabrication capabilities, we rapidly moved to fabricate almost exclusively fake-tandems (~140 substrates per day).

2.2.2. Contact layer selection and passivation layers

Beyond improved optics, e.g., via the use of textures or other optical structures, electronic losses reduce the achievable PCE of both single junction and tandem solar cells. In particular, for the widely studied perovskites in the tandem-relevant bandgap range of 1.6 - 1.7 eV, with many research groups having laid out the fundamentals bulk materials with a low bulk defect density the interfaces to and contact layers themselves require extra attention[9]. For the optically more favorable p-i-n structured perovskite solar cells the hole-transport layers compatible with random textures require additional consideration since they are likely not forming from a continuous conformal layer from solution, e.g., if based on nanoparticles or polymers. Our team has previously succeeded in forming continuous, non-dewetting HTL layers based on Spiro-TTB formed by PVD. Since this demonstration, a new class of hole-transport layers has emerged with several advantageous properties. In detail, carboxylic or phosphonic acid-bound carbazole or arylamine substitutions have been (re-) discovered for their use in perovskite solar cells. They require minimal material usage and self-organize into comparably compact self-assembled

monolayers (SAM) with widely tuneable physical and chemical properties. In particular, phosphonic acids carbazole-substituted, forming the base of the initial names (PA-Cz, phosphonic acid, carbazole, MeO-2PACz, 2PACz, Me4-PACz, …) have propelled the p-i-n devices architecture and with that the tandem devices forward. We observed similar effects for both of our perovskite fabrication methods, being fully solution or PVD+ solution, i.e., hybrid.

Exemplary, we show a loss analysis carried out to identify the recombination losses associated with the perovskite in contact with different HTL and ETL layers. We vary the HTL between spiro-TTB, TaTm and the aforementioned SAM Me-4PACz. Additionally, we assess the losses when contacting the perovskite further with the ETL (C60, thermally evaporated) and repeat both experiments with and without an additive (FBPAc). We record the photoluminescence quantum yield at one sun-equivalent illumination conditions. The PQLY serves as a proxy for the losses via $\Delta V_{OC,non-rad.} = \frac{kT}{q} \ln(PLQY)$.

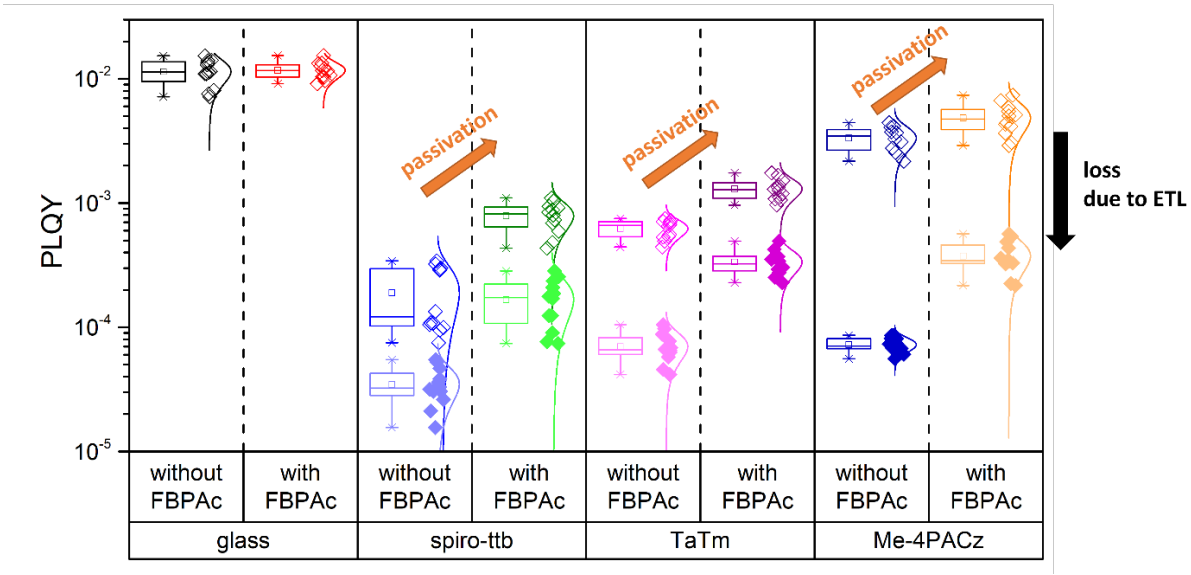


Figure 5: PLQY loss analysis for hybrid-deposited perovskite absorbers in contact with different HTLs (reference on glass, spiro-TTB, TaTm, Me-4PACz), with and without additive for passivation (FBPAc) and in contact with the ETL (C60).

In this screening we observed that combination Me-4PACz/perovskite/C60 appeared to result in the smallest losses in PLQY (photoluminescence quantum yield), on par with TaTm/perovskite/C60, Figure 5. This serves as a proxy for recombination in open-circuit conditions, but under operation the charge carriers need to be extracted so that resistive losses (e.g., because of a low mobility*carrier density relative to the layer's thickness) cause fill-factor, and thereby PCE losses. For this reason, we finally selected Me-4PACz/perovskite/C60 as the transport layer/perovskite combination due to a circa 8% absolute higher fill-factor when compared side-by-side with TaTm, Figure 6. These devices exhibited open-circuit voltages of >1.15 V (>1.85V) and fill-factors exceeding 77% (76%) in single-junction (tandem) configuration culminating in a certified efficiency > 29% mid 2021.

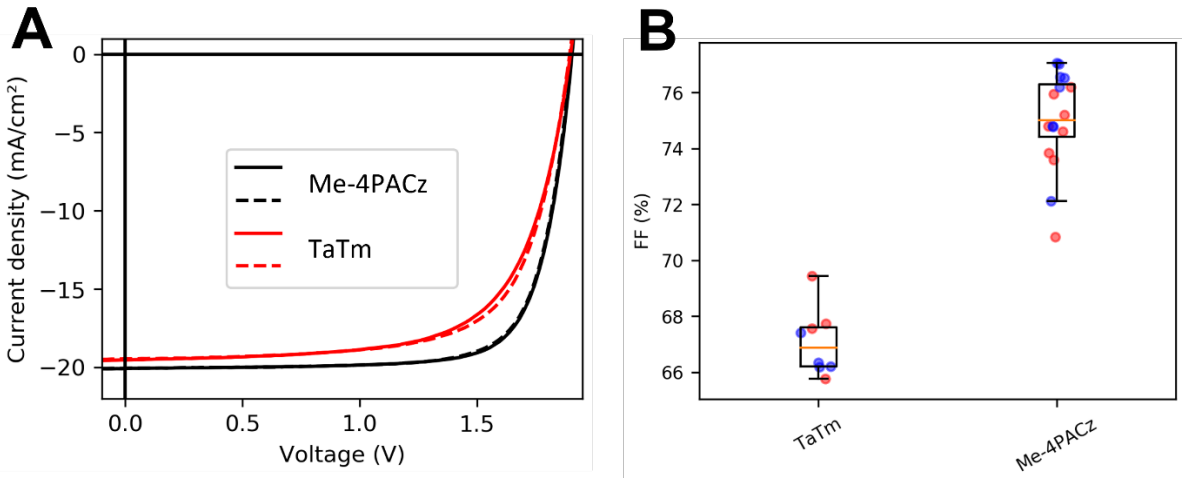


Figure 6: A) JV scans of tandem devices with a perovskite top-cell featuring TaTm or Me-4PACz as HTL in forward and reverse scan (dashed and full line, resp.). B) Fill-factor statistics of such tandem devices.

We then addressed the notoriously loss-introducing interfaces, in particular the perovskite/ETL interface.

Generally, there are three ways to reduce losses at interfaces:

- Reduce the density of defects states at said interface
- Reduce interfacial area to minimize interfacial recombination
- Limit access of minority carriers at a given interface

These concepts can be implemented by means of

- interface passivation (e.g., terminating dangling bonds)
- partial contacting
- contact displacement
- field-effect passivation

In fact, we used several of these concepts (in combination) to set a total of three world-records during a ca 6-month period,

Figure 7a.

The first approach for the fabrication of more efficient interfaces was to select a set of molecules from the vast library of molecules available and potentially previously used to terminate lead-containing materials with the highest possible surface area, thereby accentuating any surface-related effects. To this end we sought inspiration in the literature on ligands/surfactants of PbX (X = S, Se, Te) or perovskite nanocrystals. As such, we discovered phosphonic acid-based molecules that covalently bind to Pb-terminated surfaces and selected amidst them a fluoride substituted molecule so as to minimize any further interaction. Among these, FBPAc stood out with its' benzyl ring and reported passivation of perovskite nanocrystals. Indeed, admixing FBPAc to the perovskite precursor in the hybrid deposited and fully solution deposited perovskites led to a reduction in the interfacial losses in almost any configuration tested. We aimed to understand the underlying mechanism for the case of FBPAc passivation and in parallel we examined alternative interface modifications as explained below. The results are extensively shown in[11] yet in summary the crystallization of the perovskite crystal is improved resulting in better transport properties while forming insulating islands atop the perovskite which then result in a *partial contacting* scheme, thereby reducing interfacial losses (Figure 7d). We approached the loss-inducing perovskite/C60 interface simultaneously in a different study and devised a universal method to reduce the nonradiative recombination losses at that interface by depositing a conformal AlOx interlayer of just 1.5 nm via ALD, thereby *displacing the contact* interface and possibly creating a *field-effect passivation*. Notably, the precursors impact the perovskite surface if terminated with an organohalide rich surface. In contrast, when fabricating the surface to be Pb-rich by means of post-treatment (IPA wash, UV-ozone,

…) or adjusting the stoichiometry of the precursors we were able to show a 20-60 mV reduced loss in V_{OC}. Notably, this conformal dielectric layer allows for charge transport via tunnelling and hence the resistive loss it introduces is highly thickness-dependent. We therefor expanded our initial loss analyses beyond just the V_{OC},

Figure 7b. The introduction of AlOx meant a substantially reduced interface recombination, but at the same time an FF loss due to higher series resistance. These counteracting effects can be optimized by looking at the FF x V_{OC} product, which was increased by ca 60 mV in the optimized case, which means a 1% absolute efficiency gain both in single-junction devices of different bandgaps and analogously in tandem devices with a c-Si bottom cell.[12]

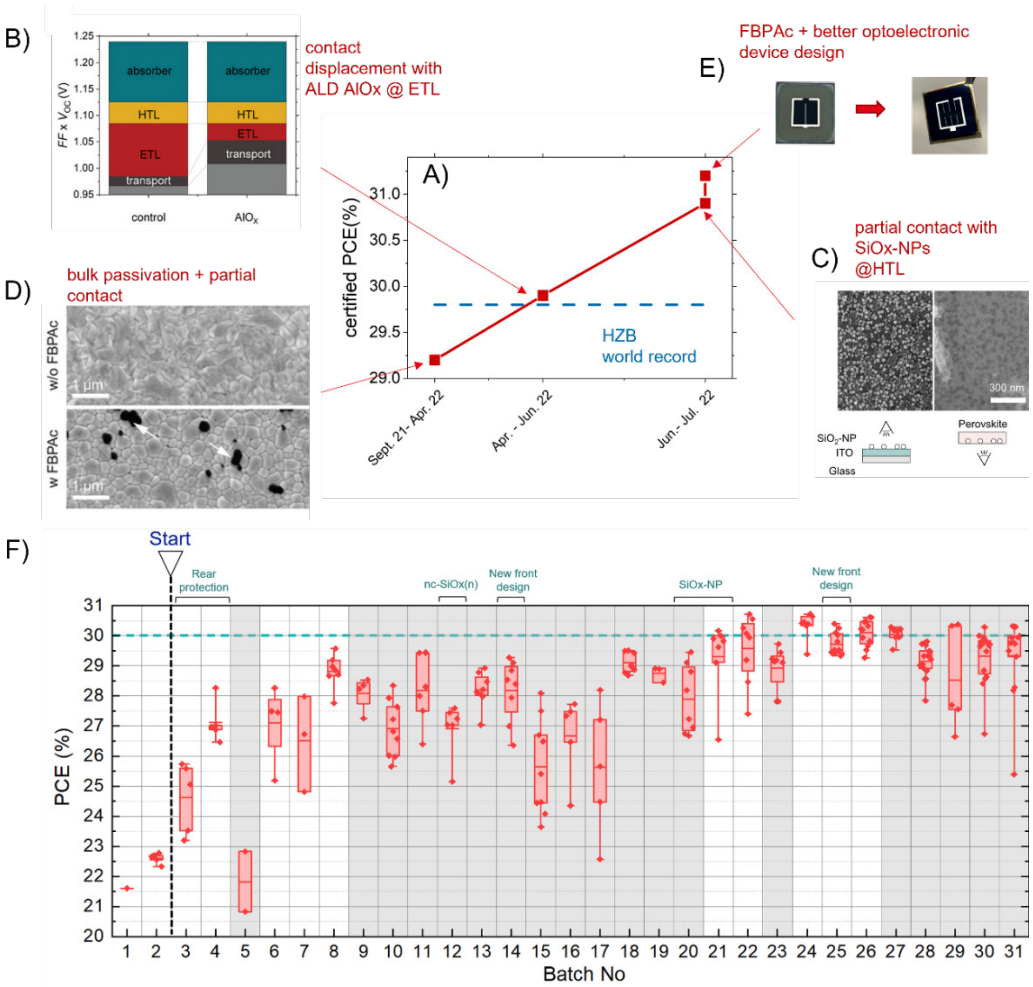


Figure 7: A) time-line of perovskite/silicon tandem solar cells fabricated by PV-LAB and certified (red) along with the world record at the time (HZB, 29.8%). The arrows around highlight some of the innovations that led to the different results. In detail: B) FF x VOC product of the perovskite top cell with and without an ALD-deposited AlOx interlayer. C) top and bottom view SEM images of SiOx nanoparticles on ITO/Me-4PACz and embedded in the peeled perovskite creating a partial contact at the HTL interface. D) bulk and interface passivation via partial contact by admixing FBPAc into the organohalide mix for creating the perovskite in a two-step method. E) Photographs with top electrode/TCO design featuring one and three fingers. F) Efficiency evolution of the front-flat tandem devices as a function of batch number highlighting the different developments. In grey are batches with known flaws (e.g., failed depositions or similar) which still allowed for overall improvements.

Me-4PACz as a HTL has enabled significant improvements for the hybrid deposited perovskites, yet for our solution-processed baseline fabrication we observed severe issues due to the hydrophobic nature of the terminating methyl-group (hence the name “Me”), not allowing us to fabricate solar cells with our standard size of 1 cm2. This effect was further amplified by the use of the previously used FBPAc as passivating additive. By introducing electronically non-active SiOx nanoparticles as wetting layer atop the Me-4PACz we were finally able to fabricate highly reproducible planar perovskite layers on top of

Me-4PACz while preserving the advantageous perovskite/C60 interface improvements. Even more so, the SiOx nanoparticles partially masked the interface between Me-4PACz and the perovskite thereby creating *a partial contact* with reduced interfacial recombination,

Figure 7c. This, together with several other smaller developments enabled the fabrication of the first ever perovskite-silicon tandem device with a certified efficiency exceeding 30%. We showcase the developments in

Figure 7f, where notably the main advancements were the introduction of a rear-protection scheme which prevented handling-induced defects, the introduction of an improved front design in two iterations, and the introduction of a new intermediate anti-reflection layer (nc-SiOx (n)) to improve light in-coupling into the bottom cell. Combining these efforts with the best top-cells we fabricated at the time (refined processing of the devices that yielded 29.2% in a hybrid deposition method) and the optimal planar solution processed top-cell yielded a double world record with certified 30.9%[13] (Figure 7c) and 31.25%[11],(Figure 7e) for the planar and fully textured cells, respectively.

These cells were subjected to different stability measurements (Figure 8) in at room temperature or elevated temperatures. Despite significant efforts the goals related to improved stability were not achieved (initial goal: *devices >30% retaining at least 90% of their initial efficiency over 1000 h of maximum power point tracking at room temperature*).

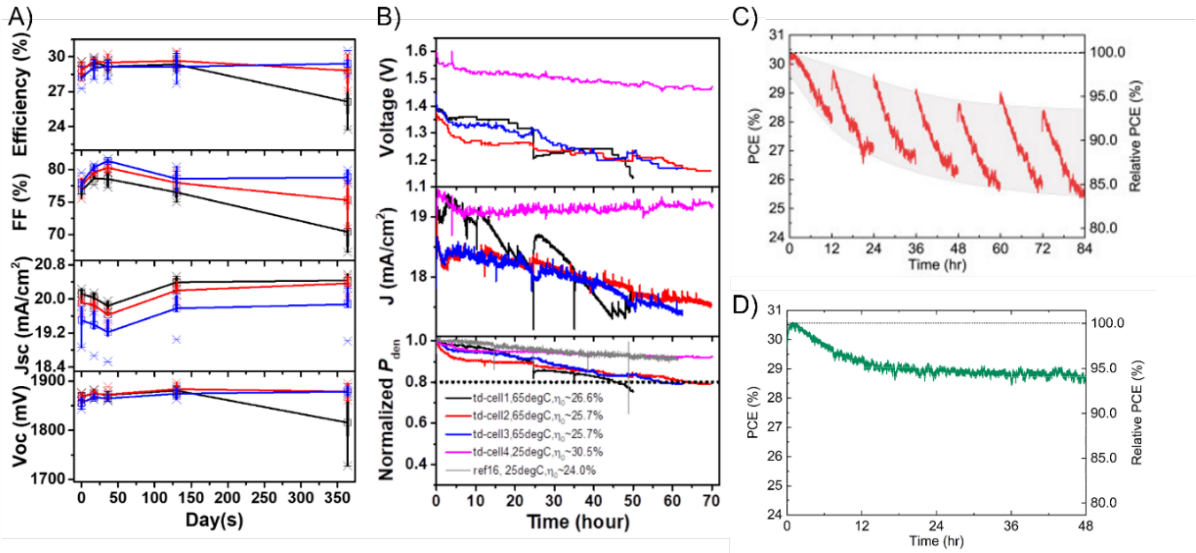


Figure 8. Stability measurements. A) storage stability (N2, dark) of fully textured tandem devices shown in some cases (here three different batches are compared) no degradation over the course of a year (red, blue) whereas others degraded slightly (black, 80% retention). B) operational stability at 25°C (pink, grey (from 2018 Nat. Mater.)) and 65°C (black, red, blue) reaching T90 of 35 and 20h at room temperature and 65°C, respectively. C) day-night cycle (12h MPP at 25°C in ambient 50% RH, 12h rest in dark at room temperature) of a front-side polished tandem. D) best continuous MPP at 25°C in ambient air with an initial burn-in for 12h and then a comparably low degradation rate of 1.2 x 10^{-4} h^{-1} corresponding to a projected T90 of ca. 830 h, assuming a linear degradation, which corresponds to only 80% of the targeted stability.

We measured the storage and power output stability of the fully textured samples (Figure 8a,b) at room temperature and at elevated temperatures (25°C and 65°C) and found that if stored in N2 the cells can maintain their efficiency over the course of a year without any losses, whereas when measured at 25°C and 65°C, the PCE drops to 90% within 75h and 25h, respectively. Similarly, when measuring the front-flat tandem devices in the ambient at a temperature of 25°C we observe a partially reversible degradation during the initial 12h of MPP tracking (Figure 8c). Similarly, for our current stability champion there is a drop of 5% rel. in the first 12h followed by a comparably slow, seemingly linear degradation with a degradation rate of 1.2 x 10^{-4}. Assuming average Swiss conditions, this would correspond to an annual

degradation rate of 4.5% abs./year, which is two orders of magnitude faster than encapsulated commercial c-Si modules. Likely, the assumption of a linear degradation is not valid but serves as a first-order approximation. It is important to note that there are several additional aspects to consider. First, our initial stability studies were carried out with unencapsulated devices. Adding glass/glass encapsulation will reduce any moisture-related degradation to a minimum and likely also slow down any egress of volatile species in the top cell. Assuming our top-cell stack is not perfectly air-tight, another degradation mode we observed is a loss in fill factor, likely due to a gradual diffusion of oxygen into the C60 ETL. Oxygen is known to create deep trap states in some organic semiconductors, including C60 and thereby reducing the electron mobility by orders of magnitude. Preventing this is critical. Similarly, the glass will attenuate parts of the ultraviolet light, preventing some of the damage it causes to the top TCO and/or the perovskite. Finally, in both cases (encapsulated and non-encapsulated) we observed a severe dependence of the tandem stability on the illumination conditions. In particular, we observed that cells with a mismatch towards the top cell being limiting retained their efficiency for a drastically longer time. This can be understood in that there is no excess carrier density (beyond the density that is being extracted) in the perovskite in operation, preventing any electrochemical side reactions.

3 Conclusions and outlook

PRESTO focused on the development of highly efficient perovskite silicon tandem solar cells. To this end, three platforms were developed that mimic the scenario in a tandem solar cell but allow for a simplified fabrication of the top cell. In particular, ZnO-modified glass was used, silicon pyramids were replicated using an NIL process, and we developed the so-called fake tandems where the silicon bottom cell serves as an electrode rather than a real bottom cell.

With the latter, different methods were screened to allow a reduction of the defect density in the bulk of the perovskite material and/or the reduction of interfacial recombination. Here, we employed different methods, such as partial contacts (SiOx nanoparticles, FBPAc), contact displacement, and field-effect passivation (AlOx). With this, it was possible to fabricate perovskite solar cells with a band gap of approximately 1.7 electron volts featuring open circuit voltages over 1.2 volts fill factors of over 80%, resulting in efficiencies above 20%.

Transferring these into tandem devices and adding several other developments that improved the optical or electric coupling of the cells (rear protection, nc-SiOx antireflection layer, and a new electrode design) enabled the fabrication off the first perovskite/silicon tandem solar cells efficiencies exceeding 30% for both a solution-processed flat top cell and a PVD-solution deposited fully textured perovskite silicon tandem.

The stability of these cells has been investigated, yet the goals that were set were not met. In particular, the best devices exhibited degradation rates, enabling a projected T90 time of approximately 830 hours. Arguably, the measurements were carried out using non-encapsulated devices so that further stability improvements are reasonable without fundamental changes to the technology itself. At the same time, the degradation rate as it presents itself currently is still approximately one order of magnitude larger than it should be for a commercial product.

With the efficiency potential being shown and further developments underway, it is critical to focus on the two remaining aspects that prevent imminent commercialization of this technology: upscale high throughput methods that are compatible with detect times in the silicon industry and further significant improvements in the operational stability in particular at elevated temperatures.

4 National and international cooperation

PV/LAB has a broad network of collaborators from academia and industry, both inside and outside Switzerland. Specifically, to this project we'd like to be mentioned the following Swiss partners:

Academic cooperations:
Empa, Groups of Sebastian Siol, Fan Fu, Romain Carron, loosely working with Yaroslav Romantschuk
ZHAW, Joint Projects with Wolfgang Tress, Beat Ruhstaller and by extension Fluxim
Haute école d'ingénierie et d'architecture de Fribourg, Jean Henneberg
EPFL, LIMNO, Kevin Sivula and LCBC, Ursula Röthlisberger
ETH Zürich, Nanomaterials Engineering Research Group, Chih-Jen Shih

Non-academic cooperations:
CSEM, Sustainable Energy Center, Headed by Prof. Ballif
Meyer-Burger Research, R&D for tandems Damien Lachenal

5 Publications and other communications

Over the course of the project, we were able to publish the results in several high-ranking peer-reviewed journals and contribute to scientific conferences and non-scientific outreach. In particular, the double world record has generated significant publicity, including several television (SRF, Eureka), radio, and newspaper (NZZ) interviews. The results from PRESTO furthermore led to one finished PhD thesis and will contribute to two more.

Main publications/ thesis:

https://www.cell.com/joule/fulltext/S2542-4351(24)00199-5
https://onlinelibrary.wiley.com/doi/full/10.1002/adma.202311745
https://pubs.rsc.org/en/content/articlehtml/2024/ee/d4ee00901k
https://www.science.org/doi/full/10.1126/science.adg0091
https://onlinelibrary.wiley.com/doi/full/10.1002/aenm.202303423
https://infoscience.epfl.ch/entities/publication/b2a7204d-83f3-4a6b-89b3-6ed00a0d8268

6 References

1. Battaglia, C., Escarré, J., Söderström, K., Erni, L., Ding, L., Bugnon, G., Billet, A., Boccard, M., Barraud, L., De Wolf, S., et al. (2011). Nanoimprint Lithography for High-Efficiency Thin-Film Silicon Solar Cells. Nano Lett *11*, 661–665. https://doi.org/10.1021/nl1037787.
2. Sahli, F., Werner, J., Kamino, B.A., Bräuninger, M., Monnard, R., Paviet-Salomon, B., Barraud, L., Ding, L., Diaz Leon, J.J., Sacchetto, D., et al. (2018). Fully textured monolithic perovskite/silicon tandem solar cells with 25.2% power conversion efficiency. Nat Mater *17*, 820–826. https://doi.org/10.1038/s41563-018-0115-4.
3. Chen, B., Yu, Z.J., Manzoor, S., Wang, S., Weigand, W., Yu, Z., Yang, G., Ni, Z., Dai, X., Holman, Z.C., et al. (2020). Blade-Coated Perovskites on Textured Silicon for 26%-Efficient Monolithic Perovskite/Silicon Tandem Solar Cells. Joule. https://doi.org/10.1016/j.joule.2020.01.008.
4. Harter, A., Artuk, K., Turkay, D., Jeangros, Q., Albrecht, S., Schlatmann, R., Ballif, C., Stannowski, B., and Wolff, C.M. (2023). Highly efficient perovskite/silicon tandem solar cells on thin nanotextured Cz-silicon bottom cells. ACS Energy Lett *in prep.*
5. Harter, A., Mariotti, S., Korte, L., Schlatmann, R., Albrecht, S., and Stannowski, B. (2023). Double-sided nano-textured surfaces for industry compatible high-performance silicon heterojunction and perovskite/silicon tandem solar cells. Progress in Photovoltaics: Research and Applications *n/a*. https://doi.org/10.1002/pip.3685.
6. Hou, Y., Aydin, E., De Bastiani, M., Xiao, C., Isikgor, F.H., Xue, D.-J., Chen, B., Chen, H., Bahrami, B., Chowdhury, A.H., et al. (2020). Efficient tandem solar cells with solution-processed perovskite on textured crystalline silicon. Science (1979) *367*, 1135–1140. https://doi.org/10.1126/science.aaz3691.
7. Boccard, M., Söderström, T., Cuony, P., Battaglia, C., Hänni, S., Nicolay, S., Ding, L., Benkhaira, M., Bugnon, G., Billet, A., et al. (2012). Optimization of ZnO Front Electrodes for High-Efficiency Micromorph Thin-Film Si Solar Cells. IEEE J Photovolt *2*, 229–235. https://doi.org/10.1109/JPHOTOV.2011.2180514.
8. Apergi, S., Brocks, G., Tao, S., and Olthof, S. (2024). Probing the Reactivity of ZnO with Perovskite Precursors. ACS Appl Mater Interfaces *16*, 14984–14994. https://doi.org/10.1021/acsami.4c01945.
9. Wolff, C.M., Caprioglio, P., Stolterfoht, M., and Neher, D. (2019). Nonradiative Recombination in Perovskite Solar Cells: The Role of Interfaces. Advanced Materials *31*, 1902762. https://doi.org/10.1002/adma.201902762.
10. Fiala, P.J. (2022). Material Development for Perovskite/Silicon Tandem Photovoltaics.
11. Chin, X.Y., Turkay, D., Steele, J.A., Tabean, S., Eswara, S., Mensi, M., Fiala, P., Wolff, C.M., Paracchino, A., Artuk, K., et al. (2023). Interface passivation for 31.25%-efficient perovskite/silicon tandem solar cells. Science (1979) *381*, 59–63. https://doi.org/10.1126/science.adg0091.
12. Artuk, K., Turkay, D., Mensi, M.D., Steele, J.A., Jacobs, D.A., Othman, M., Yu Chin, X., Moon, S., Tiwari, A.N., Hessler-Wyser, A., et al. (2024). A Universal Perovskite/C60 Interface Modification via Atomic Layer Deposited Aluminum Oxide for Perovskite Solar Cells and Perovskite–Silicon Tandems. Advanced Materials *36*. https://doi.org/10.1002/adma.202311745.
13. Turkay, D., Artuk, K., Chin, X.-Y., Jacobs, D.A., Moon, S.-J., Walter, A., Mensi, M., Andreatta, G., Blondiaux, N., Lai, H., et al. (2024). Synergetic substrate and additive engineering for over 30%-efficient perovskite-Si tandem solar cells. Joule *8*, 1735–1753. https://doi.org/10.1016/j.joule.2024.04.015.